Resonance-enhanced multiphoton ionization: Interference effects due to harmonic generation

D. J. Jackson,* J. J. Wynne, and P. H. Kes†
IBM Thomas J. Watson Research Center, P.O. Box 218, Yorktown Heights, New York 10598
(Received 30 November 1982)

A general theoretical model for the treatment of multiphoton ionization is presented. In this treatment, we have explicitly included coherent effects resulting from harmonic generation. The predictions of this model are in agreement with experimental observations that we present in this paper. In addition, the model is contrasted with much earlier theoretical treatments of multiphoton ionization and accounts for the anomalous multiphoton-ionization behavior reported by others in the literature.

I. INTRODUCTION

Most treatments of multiphoton-ionization (MPI) spectroscopy have concentrated on the effects of direct n-photon absorption[1] (where n is defined as the number of photons required to reach the ionization limit), neglecting the effects of alternate ionization channels involving parametrically generated light. In fact, a proper treatment of MPI via an intermediate resonant state $|n'\rangle$ involves the examination of all the allowed channels leading out of the resonance state as well as all of the allowed channels going into this same state. For example, the allowed channels leaving the intermediate three-photon resonant $|6s\rangle$ state in Xe I are depicted in Fig. 1(a). These are (1) continuation to five-photon ionization, (2) parametric generation, and (3) relaxation or collisional scattering to incoherent channels (radiative fluorescence, associative ionization, etc.). Clearly, the parametrically generated photon introduces more channels to the ionization continuum as shown in channel 4 of Fig. 1(a) and channels 1′—4′ in Fig. 1(b).

It may be shown that direct n-photon absorption [channel 1 of Fig. 1(a)] is not always the *only* important MPI channel in an atomic system and that there exist situations where channel 1 will not even be the *dominant* pathway to ionization. This has major implications in the general interpretation of MPI spectra, because it affects the amplitudes and line shapes of the resonances as well as the actual position of these resonances in the observed ionization signal. Specifically, there have been a number of anomalies reported in MPI spectra which are easily interpreted once all possible channels leading into and out of a resonance excitation are systematically taken into account.

In one of the earliest MPI spectra in xenon, Aron and Johnson[2] noted the absence of resonance enhancement of the lowest bound dipole transition at 68 045.67 cm^{-1} [the $5p^5\,^2P_{3/2}6s$ $J=1$ state (labeled 6s in this paper)]. In their experiment, a single dye laser at frequency ω_1 was tuned in the vicinity of one-third the frequency of the transition from the $5p^6\,^1S_0$ ground state to the 6s state, the laser beam was focused into a gas cell containing a pair of electrodes for detection of ionization, and spectra were taken for various gas pressures ~ 1 to ~ 100 Torr. Although four-photon resonance enhancement of the MPI signal due to the $5p^5\,^2P_{3/2}4f$ states were prominent in the spectra, Aron and Johnson never saw the three-photon resonance from the 6s state and saw only a weak three-photon resonance from the $5p^5\,^2P_{1/2}6s$ $J=1$ (6s′) state at low pressures ($\lesssim 1$ Torr). They remarked that "since the 6s resonance lines are so strong in one-photon absorption spectra and since three-photon transitions include the same selection rules as one-photon transitions, one would expect to see these lines prominently in the MPI spectra." In contrast to these results, working with a low-density atomic beam, Compton *et al.*[3] reported that the MPI spectrum of Xe I was dominated by a three-photon resonance due to the 6s state. Further attention was focused on this problem by Miller *et al.*[4] who studied both MPI and third-harmonic generation (THG) at $\omega_3=3\omega_1$ for several pressures of Xe I. Their observations showed a dramatic correlation between MPI and THG when the laser (ω_1) was tuned in the vicinity of the three-photon resonance with the 6s state. The strong resonance observed in the MPI signal at low pressure (<0.3 Torr) disappeared as the gas pressure increased to >1 Torr. Concurrently, THG, observed at or near resonance for the lowest pressures, shifted toward the blue (i.e., toward higher frequencies) and broadened as the pressure increased. The shift

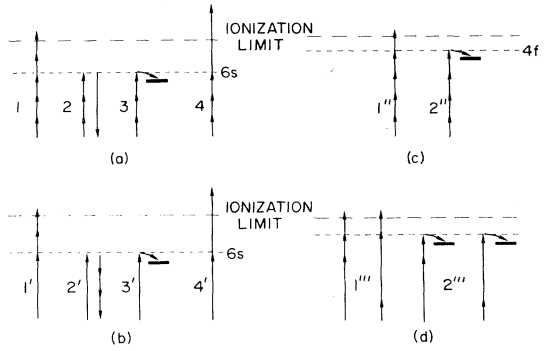

FIG. 1. Represented are the dominant pathways leading into and out of the resonant intermediate state. These are for (a) and (b) the intermediate resonant state $|n'\rangle = |6s\rangle$ and for (c) and (d) the resonant intermediate state $|4f\rangle$.

resulted in the absence of THG right on resonance for pressures greater than 1 Torr. From these results, Miller *et al.*[4] argued that "the abrupt loss of MPI signal from the 6*s* resonance can be coupled with production of intense, forward-directed, third-harmonic radiation which rapidly depletes the 6*s* state before ionization can occur." More recently, Glownia and Sander[5] have discovered a means of producing resonance enhancement *at* the position of the unperturbed 6*s* state for *all* pressures. The seemingly strange behavior reported in Xe I and other systems[4] has been the subject of detailed theoretical treatments by Payne and Garrett.[6] Their approach incorporated a time-dependent solution of a Bloch-type equation of motion for the amplitude of the resonantly excited state. Their treatment, while restricted to three-photon intermediate resonant states, is quite general in including time dependence. In contrast, we[7] have adopted a more simplified, time-independent approach, making various physically justified approximations and thereby explaining the experimental results by a relatively straightforward application of Fermi's golden rule and Maxwell's equations. We systematically included effects from all relevant channels leading up to the resonant intermediate state and focused on the interrelationship of these channels.

The format of this paper is as follows. We first present a theoretical treatment of multiphoton ionization when harmonic light is generated. In this treatment we can show that harmonic generation (HG) will have a major influence on the final ionization signal. The calculations are then experimentally verified for a three-photon intermediate resonant state in the two limits of the optically thick absorber and the optically thin absorber. In the optically thick case, we have performed a variation of Glownia and Sander's experiment and obtain results which support our theoretical predictions.[7] Systematic data taken in the optically thin medium are then presented to confirm the assertion that the HG plays an important role in the ionization process; we will discuss the broad implications of these results. In particular, the ionization behavior in the optically thin medium is dominated by the contributions of HG light and mimics the behavior of the "disappearing resonance" reported by Miller *et al.*[4]

II. THEORY

The problem under consideration is n-photon MPI of atoms in which excitation from the ground state $|g\rangle$ to an intermediate state $|n'\rangle$ coincides with the absorption of n' laser photons. Here n is defined as the number of laser photons necessary to ionize without collisional assistance, and the relation $n'<n$ is always true. The state $|n'\rangle$ is assumed to be dipole coupled to the ground state. One should distinguish between (1) a coherent virtual excitation, which results in a very definite phase relationship between the induced polarization in the medium and the driving field and (2) an incoherent excitation where these phases are random. Grischkowsky[8] presents a good physical description of how the coherent and incoherent channels are physically distinguished. The calculation of the total transition rate for the incoherent channels simply involves calculating the transition rate $1/\tau_i$ for each separate channel and then summing the individual results

$$W_{fg}^{\text{tot}}=\sum_i \frac{1}{\tau_i} .$$

With coherent excitation of the intermediate state, the electric field of the harmonically generated light $E(\omega_{2q+1},\vec{r},t)$ is intimately related (in phase as well as amplitude) to the fundamental driving field $E(\omega_1,\vec{r},t)$, and the polarization response of the medium at every point in space must reflect this relationship. To obtain a total transition rate, one must determine an *effective field* acting on the atomic dipole or correspondingly sum the transition moments acting on the ground state to $|n'\rangle$ transition.

A generalization of Fermi's golden rule for the total nth-order ionization rate in an atom sums all of the major channels (including those involving harmonically generated photons). In the electric dipole approximation, we have

$$W_{fg}^{\text{tot}}=\frac{2\pi}{\hbar^2}\rho(n\omega_1)\sum_{q=0}^{\beta} ex_{f,n-1}E(\omega_1,\vec{r},t)\left[\frac{\prod_{j=1}^{n-1}\frac{ex_{n-j,n-j-1}E(\omega_1,\vec{r},t)}{\hbar[\omega_{n-j,g}-(n-j)\omega_1]}\frac{ex_{2q+1,g}E(\omega_{2q+1},\vec{r},t)}{\hbar(\omega_{2q+1,g}-\omega_{2q+1})}}{\prod_{k=1}^{2q+1}\frac{ex_{k,k-1}E(\omega_1,\vec{r},t)}{\hbar(\omega_{kg}-k\omega_1)}}\right]^2 ,$$

$$\beta\equiv\begin{cases}\frac{1}{2}(n-1) & \text{for } n \text{ odd}\\ \frac{n}{2}-1 & \text{for } n \text{ even}\end{cases} , \quad \omega_{2q+1}\equiv(2q+1)\omega_1 . \tag{1}$$

We have defined the ground state as $|n-j-1=0\rangle=|k-1=0\rangle=|g\rangle$ and the final state as $|n\rangle=|f\rangle$. In addition, $\rho(n\omega_1)$ is the density of final states in the continuum, $x_{k,k-1}=\langle k|x|k-1\rangle$, $\omega_k=k\omega_1$, $E(\omega_k,\vec{r},t)$ is the electric field polarized in the x direction, $\omega_{kg}=\omega_k-\omega_g-i\Gamma_{kg}/2$, $\Gamma_{kg}/2$ is the linewidth, and $\hbar(\omega_k-\omega_g)$ is the energy of the nth state relative to the ground state. The sum over q determines the contributions from the different harmonics; $2q+1$ gives the order of the harmonic and is summed only over those states that are on or near resonance with a dipole-allowed transition. We have not included other permutations of the time-ordered Feynman diagrams[9] that correspond to nonresonant excitation channels since they are often negligible and may be ignored. Figures 1(a)–1(c) are examples of a single resonantly enhanced ordering of the three-, one-,

and four-photon channels, respectively. When necessary, the other permutations of the time ordering must be explicitly added to the sum in Eq. (1). Thus the 2! possible time-ordered permutations of the two-photon resonance-enhanced channels leading into the $|4f\rangle$ state shown in Fig. 1(d) are of comparable strength and must be included in Eq. (1). The reader is therefore cautioned to ascertain that all other permutations of the time orderings are *really* negligible before applying Eq. (1) verbatim.

Next, one must determine the magnitude and phase of $E(\omega_{2q+1},\vec{r},t)$, for each harmonic component. From Maxwell's equations,

$$\vec{\nabla}\times\vec{\nabla}\times\vec{E}(\omega_{2q+1},\vec{r},t)+\frac{1}{c^2}\frac{\partial^2}{\partial t^2}\vec{D}(\omega_{2q+1},\vec{r},t)=0\ , \tag{2}$$

where $\vec{D}=(\vec{E}+4\pi\vec{P}^{\,\mathrm{tot}})\hat{x}$ and P^{tot} will include both a linear term and a nonlinear source term[10] $P^{\mathrm{NLS}}((2q+1)\omega_1,\vec{r},t)$ defined as

$$P^{\mathrm{NLS}}((2q+1)\omega_1,\vec{r},t)=\tfrac{1}{4}N_0\chi^{(2q+1)}((2q+1)\omega_1)E^{(2q+1)}(\omega_1,\vec{r},t)\ , \tag{3}$$

with N_0 the atomic density and $\chi^{(2q+1)}((2q+1)\omega_1)$ the $(2q+1)$th-order nonlinear susceptibility. Again all permutations of the time-ordered Feynman diagrams for $(2q+1)$th-harmonic generation[9] should be used to calculate the $(2q+1)$th-order nonlinear susceptibility, but only the dominant terms (those for which the denominators are resonant) are kept.

The xenon $6s$ and $4f$ states have been investigated experimentally, by us and others.[2–7] The wealth of available xenon data makes it convenient to use this specific case to demonstrate the approach to the more general problem. We have therefore sketched in Figs. 1(a) and 1(b) all possible channels for exciting the xenon $6s$ state with $n=5$ and the intermediate $|6s\rangle$ state near resonance with three laser photons. The first step to ionization is defined as a coherent virtual excitation [represented by the short-dashed line in Fig. 1(a)] of the $6s$ state by three laser photons at ω_1 [solid arrows in Fig. 1(a)]. The second step, after excitation, is one of these three possible channels leaving the virtual state: (1) the absorption of two additional photons to ionize, (2) parametric fluorescence or THG, and (3) collisional scattering to the $6s$ incoherent state or radiative relaxation. (The convention here will be to use an arched arrow going into a solid bar to denote all the incoherent channels.) Clearly, the generated third-harmonic photon from channel 2 can also induce a parallel excitation to the coherent virtual state followed by branching into the same three outgoing channels, as shown in Fig. 1(b). A fourth channel (the absorption of a THG photon in the second step to ionization) is also shown, but the contributions from channels 4 and 4′ effectively represent higher-order processes[11] in xenon and are negligible. They are included here to remind the reader that if more than six photons are required to reach the ionization limit and the second step is resonant, these two channels and their ensuing family of associated diagrams would have to be included in Eq. (1). [Caution: These permutations have not been explicitly included in the summations of Eq. (1).] Note that channels 1 and 1′ are coupled via channels 2 and 2′, but $E(\omega_3,\vec{r},t)$ is roughly five orders of magnitude smaller than $E(\omega_1,\vec{r},t)$ so that the coupling via channel 2′ can be ignored. The ensuing calculation will concentrate on defining the interdependence of the remaining terms. From Eq. (1) the fifth-order transition rate is

$$W_{fg}^{\mathrm{tot}}(5\omega_1,\vec{r},t)=\frac{2\pi}{\hbar^2}\rho(5\omega_1)\left|\sum_k\frac{ex_{fk}E(\omega_1,\vec{r},t)ex_{kn'}E(\omega_1,\vec{r},t)}{\hbar(\omega_{kg}-4\omega_1)\hbar(\omega_{n'g}-3\omega_1)}\langle n'|ex\,\mathcal{F}^{T}(3\omega_1,\vec{r},t)|g\rangle+ex_{fg}E(\omega_5,\vec{r},t)\right|^2\ , \tag{4a}$$

where

$$\langle n'|ex\,\mathcal{F}^{T}(3\omega_1,\vec{r},t)|g\rangle\equiv\sum_{m,m'}\frac{ex_{n'm}E(\omega_1,\vec{r},t)ex_{mm'}E(\omega_1,\vec{r},t)ex_{m'g}E(\omega_1,\vec{r},t)}{\hbar(\omega_{mg}-2\omega_1)\hbar(\omega_{m'g}-\omega_1)}+ex_{n'g}E(\omega_3,\vec{r},t)$$

$$=ex_{n'g}[E_{\mathrm{eff}}(3\omega_1,\vec{r},t)+E(\omega_3,\vec{r},t)]\ . \tag{4b}$$

(Remember that $n'=3$ and $|n'\rangle\equiv|6s\rangle$.) Under our experimental conditions in the low-density limit, collisional scattering to an incoherent excitation of the $6s$ state is expected to have a small effect on the coherent excitation. The relaxation and scattering losses are included in the imaginary part of the energy denominators. The terms which affect the $|6s\rangle$ to $|g\rangle$ transition are grouped together in Eq. (4b) as

$$\langle 6s|ex\,\mathcal{F}^{T}(3\omega_1,\vec{r},t)|g\rangle\ .$$

The coherent sum $\mathcal{F}^{T}(3\omega_1,\vec{r},t)$ thus represents the *net effective transverse field* acting on the ground state to $|6s\rangle$ transition. Here $E_{\mathrm{eff}}(3\omega_1)$ represents an effective field which drives the transition at $3\omega_1$. The coupling relation between the THG field $E(\omega_3,\vec{r},t)$ and the laser field $E(\omega_1,\vec{r},t)$ can then be calculated from the wave equation [Eq. (2)],

$$\vec{\nabla}\times\vec{\nabla}\times\vec{E}(\omega_3,\vec{r},t)-\epsilon_3\left[\frac{\omega_3}{c}\right]^2\vec{E}(\omega_3,\vec{r},t)$$

$$=4\pi\frac{\omega_3^2}{c^2}\vec{P}^{\,\mathrm{NLS}}(3\omega_1,\vec{r},t)\ , \tag{5}$$

where ϵ_i is defined as the linear dielectric constant at ω_i.

For this calculation, we assume a focused geometry for the laser beam, with confocal parameter $b=2\pi w_0^2/\lambda=2\lambda f^2/\pi\,(w_f)^2$ (see Ref. 12) where w_0 is the waist in the focus, w_f is the waist at the lens, and f is the focal length of the lens. We also assume low densities and low laser powers but will later show that the ensuing results are valid even with pronounced pressure- and power-broadening effects. There are two limits where this calculation is easily performed, first if the absorber is optically thick at the third-harmonic frequency ω_3, and second when the absorber is optically thin at ω_3. In both cases, the medium is considered to be nonabsorbing at the fundamental frequency ω_1.

A. Optically thick absorber

In this calculation, the optically thick absorber is defined as a system where the absorption depth at ω_3 is much shorter than the length of the sample. Further, if the laser beam is tightly focused, the length of the sample is effectively given by the confocal parameter of the beam. Over this distance, there is no appreciable change in the beam intensity; it therefore follows that the change in intensity at ω_1 over an absorption depth is negligible. Thus $E(\omega_1,\vec{r},t)$ and $E(\omega_3,\vec{r},t)$ can be conveniently approximated by plane waves and we will seek a plane-wave solution to Eq. (5) with

$$E(\omega_1,\vec{r},t)=\frac{E(\omega_1)}{2}e^{i(k_1z-\omega_1t)}+\text{c.c.}$$

Physically, having an optically thick medium means that the third-harmonic field strength reaches a steady-state value after propagating an absorption depth into the material. We will now derive the steady-state solution for a plane-traveling wave in the medium where the driving polarization is

$$P^{\text{NLS}}(3\omega_1,\vec{r},t)=\tfrac{1}{2}P^{\text{NLS}}_{\text{trav}}(3\omega_1)e^{i(3k_1z-3\omega_1t)}+\text{c.c.}$$

The general solution to the wave equation is

$$E(\omega_3,\vec{r},t)=\{[E_{\text{trav}}(\omega_3)/2]e^{i(3k_1z-3\omega_1t)}+(A_{\text{trav}}/2)e^{i(k_3z-\omega_3t)}\}+\text{c.c.}\,, \tag{6}$$

where $k_i=\epsilon_i^{1/2}\omega_i/c$, $E_{\text{trav}}(\omega_3)$ is the amplitude of the particular solution (i.e., the driven response which propagates at $c/\epsilon_1^{1/2}$), and $A_{\text{trav}}(\omega_3)$ is the amplitude of the homogeneous solution (i.e., the natural solution to the wave equation which propagates at $c/\epsilon_3^{1/2}$).[10] In the optically thick absorber, the homogeneous solution is strongly attenuated by the imaginary part of k_3, so that only the driven term $E_{\text{trav}}(\omega_3)$ survives beyond an absorption depth. Solving Eq. (5) for the particular solution gives

$$E_{\text{trav}}(\omega_3)=4\pi P^{\text{NLS}}_{\text{trav}}(3\omega_1)/(\epsilon_1-\epsilon_3)\,. \tag{7}$$

It is important to note that this solution together with Eqs. (3) and (6) establishes a *constant phase* relationship between $E(\omega_3,\vec{r},t)$ and $E^3(\omega_1,\vec{r},t)$.

The nonlinear source term is related to the laser field $E(\omega_1,\vec{r},t)$ through the nonlinear response of the medium. From Eq. (3)

$$P^{\text{NLS}}_{\text{trav}}(3\omega_1)=\frac{\chi^{(3)}(3\omega_1)}{4}E_1^3(\omega_1)=\frac{N_0e^4}{4\hbar^3}\left[\sum_{m,m'}\frac{x_{gn'}x_{n'm}x_{mm'}x_{m'g}}{(\omega_{n'g}-3\omega_1)(\omega_{mg}-2\omega_1)(\omega_{m'g}-\omega_1)}\right]E^3(\omega_1)\,. \tag{8}$$

Furthermore, when the only resonant contribution to the linear susceptibility is the ground state to $|6s\rangle$ transition, then

$$\epsilon_1-\epsilon_3\cong-\frac{4\pi N_0e^2|x_{n'g}|^2}{\hbar(\omega_{n'g}-\omega_3)}\,. \tag{9}$$

This expression is complex because $\omega_{n'g}$ contains an imaginary damping term. Substituting Eqs. (8) and (9) into Eq. (7) yields

$$ex_{n'g}E_{\text{trav}}(\omega_3)=-\frac{[ex_{n'm}E(\omega_1)][ex_{mm'}E(\omega_1)][ex_{m'g}E(\omega_1)]}{(\omega_{mg}-2\omega_1)(\omega_{m'g}-\omega_1)}=-ex_{n'g}E_{\text{eff}}(3\omega_1)\,. \tag{10}$$

Astonishingly, in the optically thick absorber $E_{\text{trav}}(\omega_3)$ is 180° out of phase with respect to $E^3(\omega_1)$.

Furthermore, third-harmonic generation with traveling-wave excitation in the optically thick absorber is the special case where these channels 1 and 1′ have *exactly* the same magnitude. This comes about because the denominator in Eq. (7) removes the dependence of $ex_{n'g}E_{\text{trav}}(\omega_3)$ on the dipole matrix element $|x_{n'g}|$ and resonant denominator $\omega_{n'g}-\omega_3$. Thus the two terms $E_{\text{eff}}(3\omega_1)$ and $E_{\text{trav}}(\omega_3)$ exactly cancel and $\mathcal{F}^T(3\omega_1)$ in Eq. 4(b) is zero. [Note that the normalization occurs *independent* of the size of the linewidth factor $\Gamma_{n'g}$ such that extra contributions to the linewidth from power broadening or pressure broadening will not affect the result in Eq. 4(b).]

This leaves the ionization process dependent upon the generation of the fifth harmonic $E(\omega_5,r,t)$. From Eqs. (2) and (3) one can determine the amplitude of the fifth harmonic

$$E_{\text{trav}}(\omega_5)=\frac{4\pi P^{\text{NLS}}_{\text{trav}}(5\omega_1)}{\epsilon_1-\epsilon_5}$$

with

$$P^{\text{NLS}}_{\text{trav}}(5\omega_1)\equiv\frac{\chi^{(5)}}{16}E^5(\omega_1)+\frac{\chi^{(3)}}{4}E_{\text{trav}}(\omega_3)E^2(\omega_1)\,.$$

At our experimental pressures, the gas is optically thin for

the fifth harmonic (i.e., the absorption depth is always greater than the confocal parameter). The same resonant terms which enhance THG also make the dominant contributions to fifth-harmonic generation and these terms cancel in the same manner as $\mathcal{F}^T(3\omega_1)$; very little fifth harmonic will be generated, and $ex_{fg}E(\omega_5,\vec{r},t)$ in Eq. (4a) may be neglected[13] (see the Appendix).

As a consequence, the resonance-enhanced multiphoton-ionization rate calculated by Eq. (4a) is zero since the net effective transverse field in Eq. (4b) vanishes. The expression $\mathcal{F}^T(3\omega_1)$ takes on physical meaning when one realizes that the transverse component of the polarization pseudovector (defined in the two-state vector model[14]) is proportional to $\mathcal{F}^T(3\omega_1)$ under conditions of adiabatic following. In terms of this vector model, when $\mathcal{F}^T(3\omega_1)$ vanishes the pseudovector is forced to point straight down by the dynamic balance of the two forces that are driving the ground state to $|6s\rangle$ transition 180° out of phase. No work is done by the fields to polarize the medium at ω_3, meaning that in the steady state there is no coherent superposition of the ground state to $|6s\rangle$ transition. As a consequence, the population stays in the ground state. While there may be short-range fluctuations of this pseudovector from the zero point, over an absorption depth, these fluctuations damp out. Figure 2(a) depicts the response of $\vec{p}$, the pseudovector of the two-state vector model, to the net effective transverse field applied to the ground state to $|n'\rangle \equiv |6s\rangle$ transition at ω_3. For traveling-wave excitation, the net effective field is zero because the field at ω_3 and the effective field at $3\omega_1$ are of equal magnitude but 180° out of phase.

There is another physically significant dimension in this problem. It is the coherence length for THG, which is defined as the intrinsic distance over which the fields $E(\omega_1,\vec{r},t)$ and $E(\omega_3,\vec{r},t)$ travel before getting out of phase, i.e., $l_{\rm coh}=|\pi/\Delta k|=|\pi/(3k_1-k_3)|$. In the above calculation for a traveling-wave excitation, the coherence length is limited by the absorption depth when the absorption depth is shorter than the length of the sample.

Writing Eq. (7) in terms of the coherence length of the sample,

$$|E_{\rm trav}(\omega_3)|=\left|2\left[\frac{\omega_3}{c}\right]^2 l_{\rm coh}P^{\rm NLS}_{\rm trav}(3\omega_1)\right|, \tag{11}$$

gives a third-harmonic field strength $E_{\rm trav}(\omega_3)$ which is directly proportional to this physical parameter. When $l_{\rm coh}$ is *equivalent* to the absorption depth, the dynamic balance between $E_{\rm trav}(\omega_3)$ and $E_{\rm eff}(3\omega_1)$ is achieved, $\mathcal{F}^T(3\omega_1)=0$, and the medium is depolarized. Changing the coherence length with respect to the absorption depth will destroy the dynamic balance which depolarizes the medium thereby allowing one of the channels to dominate the ionization process. For example, with standing-wave excitation[7] the driving polarization has the form

$$\begin{aligned}P^{\rm NLS}(3\omega_1,\vec{r},t)&=P^{\rm NLS}_{\rm stand}(3\omega_1)[\cos(k_1z)]^3e^{-i3\omega_1t}+\text{c.c.}\\&=\tfrac{1}{4}P^{\rm NLS}_{\rm stand}[\cos(3k_1z)+3\cos(k_1z)]e^{-i3\omega_1t}+\text{c.c.}\end{aligned} \tag{12}$$

For this nonlinear polarization, the solution of the wave equation

$$\begin{aligned}|\vec{E}_{\rm stand}(\omega_3,\vec{r},t)|&=\pi P^{\rm NLS}_{\rm stand}(3\omega_1)\left[\frac{\cos(3k_1z)}{\epsilon_1-\epsilon_3}+\frac{3\cos(k_1z)}{\epsilon_1/9-\epsilon_3}\right]\\&=\frac{1}{2}\left[\frac{\omega_3}{c}\right]^2 P^{\rm NLS}_{\rm stand}(3\omega_1)[l^{3k_1}_{\rm coh}\cos(3k_1z)+3l^{k_1}_{\rm coh}\cos(k_1z)e^{i\phi}]\end{aligned} \tag{13}$$

shows that the Fourier component of the source term at $3k_1$ still generates a third-harmonic field whose polarization field cancels that of the driving term. (The relative phase ϕ changes as one tunes through resonance.) Here, in contrast to the traveling-wave case, the Fourier component at k_1 has a shortened coherence length (which is comparable to one wavelength) and does not produce enough third harmonic to cancel out the effect of the driving term at k_1. Via this k_1 term, five-photon absorption dominates the ionization channels when standing-wave excitation is used. This of course assumes the absorption depth is longer than the laser wavelength. In terms of the two-state vector model[14] for the response of the medium, the standing-wave field induces a polarization on the ground state to $|n'\rangle$ transition, causing the pseudovector to tip away from the z axis as shown in Fig. 2(b). Note that for the *linearly polarized* standing-wave excitation, *some* third harmonic is still generated causing destructive interfer-

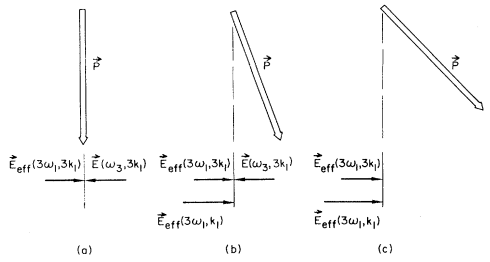

FIG. 2. Response of the pseudovector from the two-state vector model to the applied transverse effective fields in the optically thick absorber. Shown below are the magnitudes of the driving fields for (a) linearly polarized traveling-wave excitation, (b) linearly polarized counterpropagating beams, and (c) circularly polarized counterpropagating beams of the same sense.

ence, but the destructive interference is *not* complete. In contrast, the experimental configuration of Glownia and Sander,[5] using circularly polarized counterpropagating beams, produced *no* third harmonic. This is illustrated in Fig. 2(c) where the polarization of the medium at ω_3 is shown to be completely unattenuated and ionization via channel 1 dominates.

B. Optically thin absorber (off-resonance ionization)

Channel 1′ can dominate the ionization process when one tunes far enough off resonance for the absorption depth to become longer than the length of the sample. In this limit, the Gaussian nature of the beam and the phase relationship of the free wave (the homogeneous solution) become important. The Gaussian waveform complicates the evaluation of Maxwell's equations; this is because the phase of $E(\omega_3,\vec{r},t)$ now *changes* with respect to $E^3(\omega_1,\vec{r},t)$ at every point in space. Even so, they are still coherently related, and the evolution of this problem involves integrating the phase contributions throughout the sample volume; though nontrivial, it has been solved in the familiar treatment of THG generation from a well-defined Gaussian beam.[15] The ionization rate $W^{\rm tot}(5\omega_1)$ for the optically thin absorber may then be written in terms of the third-harmonic intensity[1]:

$$W_{fg}^{\rm tot}(5\omega_1)\cong W_{fg}^{(3)}(\omega_3,2\omega_1)=2\pi\rho(\omega_3,2\omega_1)\left[\frac{2\pi\alpha}{\hbar}\right]^3 I_1^2 I_3\left|\sum_{kk'}\frac{x_{fk}x_{kk'}x_{k'g}}{(\omega_{kg}-\omega_3-\omega_1)(\omega_{k'g}-\omega_3)}\right|^2, \tag{14}$$

where $I_i=(c/8\pi)[E(\omega_i)]^2$ and $\alpha=e^2/\hbar c$ is the fine-structure constant. The motivation for writing Eq. (14) in this form is that it allows one to compare experimental measurements $W_{fg}^{\rm tot}(5\omega_1)$ and I_3 as a function of frequency.

Furthermore, the THG intensity I_3 shows strong characteristic dependencies on other experimental parameters. Varying these parameters should thus allow us to vary the ionization behavior according to the prescriptions of Eq. (14). Previous theoretical and experimental findings of THG are summarized as follows: THG via the $6s$ state in xenon is always generated on the short-wavelength side of the atomic resonance. It is expected to have a cubic dependence on the laser intensity I_1^3, thus the overall power dependence of $W_{fg}^{\rm tot}(5\omega_1)$ will be I_1^5. THG will also exhibit a strong functional dependence on the density of the gas and the focusing geometry of the beam (the confocal parameter). Specifically, increasing either the atomic density or the confocal parameter will alter the optimum phase-mismatch condition, causing the peak of the THG spectrum to shift to shorter wavelengths. Bjorklund[15] has generated computer plots which summarize the THG behavior with changing pressure and confocal parameters.

III. EXPERIMENTAL SETUP

In these experiments, the output of a Quanta Ray Nd:YAG pumped dye laser was focused into a low-pressure xenon cell (Fig. 3). Using Coumarin 440 as an active medium and pumping with moderate powers of the Nd:YAG third harmonic (355 nm) yielded typical output intensities of 110 kW with dye-laser linewidths of 0.3 $\rm cm^{-1}$. The measured dye-laser pulse length was 4 nsec. The laser intensity was monitored at the laser output by picking off a small fraction of the intensity with a beam splitter and sending it to a biplanar diode whose output was averaged on a gated integrator. In the spectra, we calibrated the separation between the $6s$ and $4f$ resonances by inserting an etalon before the biplanar diode to provide 2.5-$\rm cm^{-1}$ frequency markers. The ionization detector consisted of a pair of plates spatially separated by 1.0 cm, one of which was held at $+260$ V while the other was used to measure the ionization current. The ionization signal was generally amplified before being integrated, digitized, and recorded on a computer through a device-coupling interface. The output of the integrator was simultaneously displayed on a strip chart recorder.

An absolute wavelength calibration was important to determine the magnitude of the Stark shifts for the two resonances. The beginning of each scan was digitally reset at 441.06 ± 0.02 nm. This wavelength was determined by a Jarrel Ash 0.5-m spectrometer which in turn was calibrated against three emission lines from a mercury lamp.

Figures 4(a)—4(c) depict the three different experimental configurations of cells used in these measurements. For the standing-wave measurements, we used the single-cell arrangement shown in Fig. 4(a) where the lens was fixed with its axis parallel to the long dimension of the plate so that the focus of the lens fell near the center of the 30-cm-long gas cell. A second lens and mirror retroreflected and refocused the laser light back into the cell, creating a standing-wave excitation. The traveling-wave spectra were obtained by blocking the retroreflecting mirror. To study the case of the optically thin absorber, a solar blind EMI CsI photomultiplier replaced the lens and mirror at the output of the xenon cell [Fig. 4(b)] and was used to monitor the generation of third-harmonic light in the forward direction. To prevent absorption by oxygen of the vacuum-ultraviolet (vuv) light at 146.9 nm, a lithium

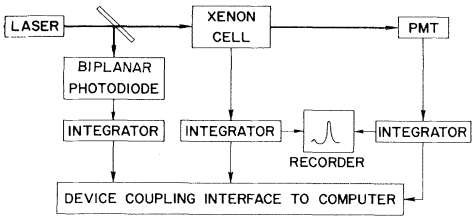

FIG. 3. Schematic of the experimental setup.

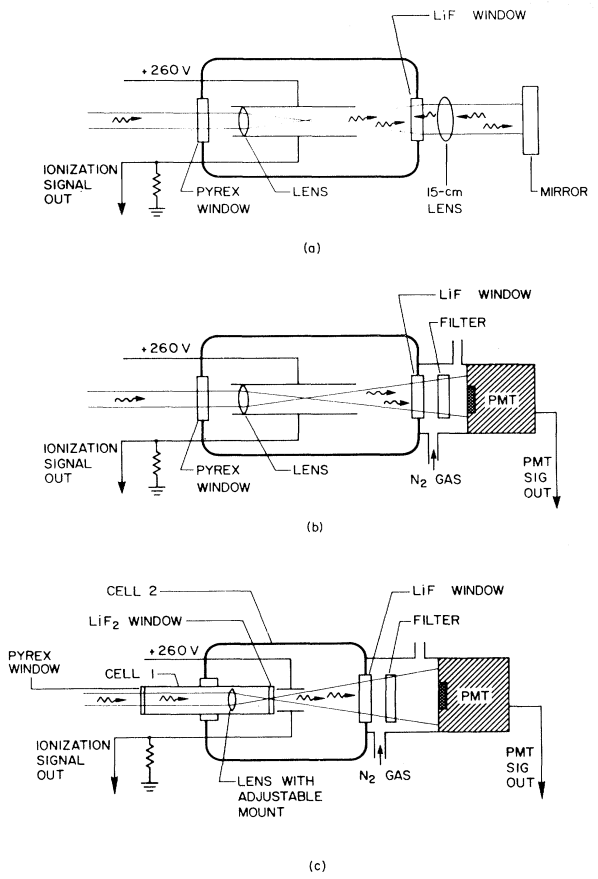

FIG. 4. Details of ionization chamber configurations. (a) Ionization detection of retroreflected laser pulse, (b) ionization detector with PMT to simultaneously monitor THG signal, and (c) double-cell experiment where THG is generated in cell 1 and three-photon ionization is detected in cell 2.

fluoride exit window was used, and the volume between the cell and the photomultiplier was flushed with dry nitrogen. A narrow-band filter (Acton Research) with a 27-nm pass band and a peak transmission at 134.9 nm was also placed before the photomultiplier to attenuate the blue laser light. The photomultiplier output signal was then integrated and sent to the computer and strip chart recorder.

Measurements were taken using lenses with focal lengths of 1.0, 1.8, 2.7, and 8.0 cm. The first three lenses were mounted inside of the gas cell in the space separating the ionization probes. The longer, 8-cm focal length lens was mounted in a special holder and adjusted so that its focus fell between the plates. The confocal parameters, as determined by the relation $b=2\pi w_0^2/\lambda$, where w_0 is the beam waist at the focus, are estimated to be 30 μm, 50 μm, 200 μm, and 2 mm, respectively. (In this discussion these values for the confocal parameters are used to connote a rough measure of the sample length over which the MPI and THG take place. It should be understood, however, that the laser beam in our experiments was not single mode, hence the numbers quoted are very rough estimates.) Measurements taken at the 2-mm confocal parameter differ in that the plate voltage in the ionization chamber was $+30$ V instead of 260 V and the outgoing signal was amplified by an additional factor of 10.

To monitor the ionization generated outside of the beam focus (where there are no high-field intensities to distort the line shapes), we used a double-cell experimental arrangement. As shown in Fig. 4(c) two pressure-isolated cells were used; the generation of the vuv light occurred in cell 1 while the ionization signal from the unfocused vuv light was observed in cell 2. Reabsorption of the vuv light within the first cell was minimized by placing the focused waist of the beam as close as possible to the lithium fluoride window which separates the two cells. The absorption path between the two lithium fluoride windows of the second cell was 21 cm. Again, the volume between the output window of the cell and the photomultiplier was steadily flushed with nitrogen gas to prevent absorption of the vuv light. The peak wavelength of the vuv spectrum was tuned by varying the pressure in the first cell.

IV. RESULTS

Five sets of experiments were performed. Experiment I exemplifies the expected behavior in the optically thick absorber under both standing-wave and traveling-wave excitation. The other four experiments, carried out with traveling-wave excitation, test the prediction that reabsorption of the parametrically generated wave makes an important and observable contribution to ionization. This was accomplished in experiments II and III by varying the experimental parameters which would most strongly affect the THG. Experiment IV confirms the expected power dependence. Finally, in experiment V we unambiguously demonstrate the existence of the three-photon ionization channel.

A. Experiment I. Optically thick absorber

In a variation of Glownia and Sander's experiment[5] [Fig. 4(a)] we used a glan prism polarizer to *linearly* polarize the input beam. This experiment demonstrated that the ionization behavior expected from our calculations in Sec. II is easily observed for both traveling- and standing-wave excitation of the sample with linearly polarized light. Figure 5 depicts the behavior of a pair of scans taken for $b=300$ μm at 1.5 Torr. The figure on the left represents the ionization signal resulting from traveling-wave excitation, while that on the right shows the ionization signal when a standing wave is induced in the cell. In these spectra, the $4f$ resonance signal is always included as a reference against which to judge the behavior of the $6s$ resonance since, as will be discussed later, the $4f$ is not as strongly affected by interference phenomena. There was no observable resonance at the unperturbed $6s$ state when traveling-wave excitation was used, but with standing-wave excitation a strong ionization signal at the unperturbed $6s$ resonance position is dramatically evident.

The $6s$ resonance induced by the standing-wave field exhibits the asymmetric line profile characteristic of the Stark broadening and shifting expected in this state.[16,17] The 4-cm^{-1} width of this transition is in order-of-magnitude agreement with an estimate based on the known oscillator strength for this transition and a laser in-

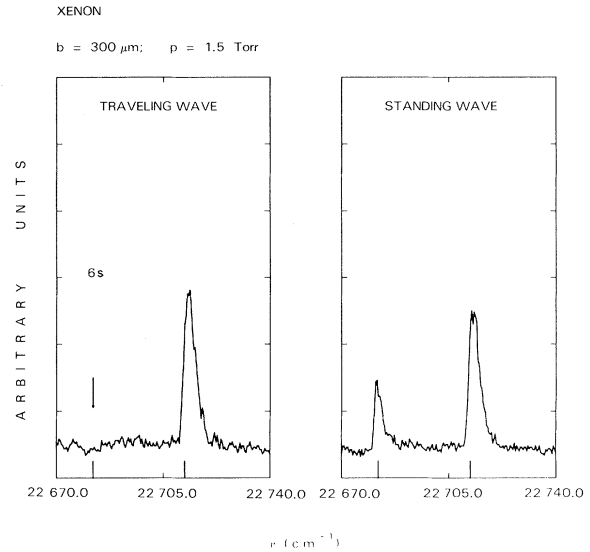

FIG. 5. These figures summarize the results of our measurements in the optically thick case. Ionization signal for traveling-wave excitation (curve on the left) and standing-wave excitation (curve on the right). They demonstrate the sudden appearance of resonance enhancement via the $|6s\rangle$ state after a net dipole is induced in the medium by standing-wave excitation.

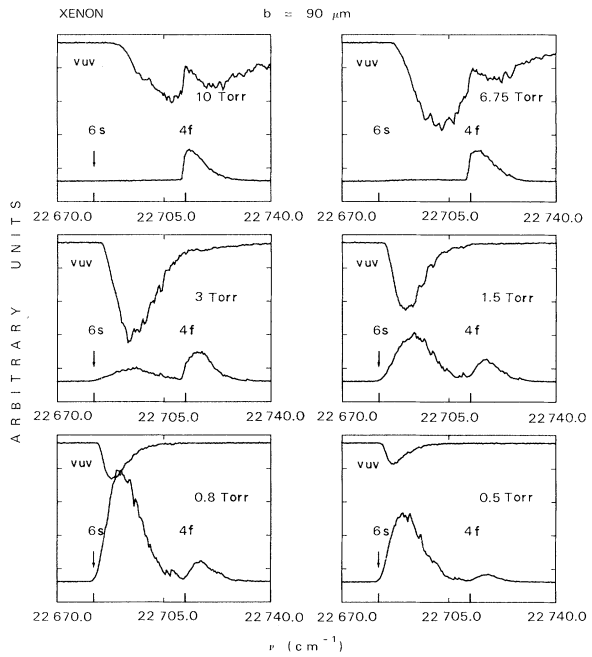

FIG. 6. To test the behavior of MPI in the optically thin medium, the measured pressure dependence of THG (upper curve) and ionization signal (lower curve) vs laser energy in cm^{-1} are shown. Plate voltage, preamplifier gain, and PMT voltage were constant for all six measurements. Tick marks indicate the positions of the unperturbed $6s$ and $4f$ states and PMT and ion chamber sensitivities are constant for all measurements. Note that the "$6s$" excitation requires the presence of THG near the enhancing resonance. Within the Lorentzian linewidth, ionization is suppressed by the depolarization effect.

tensity of 10^{11} W/cm^2. It is also in good agreement with the ~ 5-cm^{-1} shift observed by monitoring the fluorescence at right angles to the direction of an exciting laser beam of the same intensity.[17]

It should be emphasized that in our measurements, the counterpropagating beams are linearly polarized in the same sense. On the other hand, if the retroreflected beam is polarized perpendicular to the incident beam, no resonance enhancement at the $6s$ state is observed.[18] The S to P transition is the special case where the sum of the quantum-mechanical amplitudes for counterpropagating orthogonally polarized beams is zero.[19]

To demonstrate that the appearance of the $6s$ resonance is not a consequence of doubling the laser intensity upon reflection, the laser intensity was attenuated by 40%, whereupon we *still* found strong ionization via the $6s$ state under conditions of standing-wave excitation. We note that good spatial overlap of the counterpropagating beam in these measurements is very critical. Finally, a parallel set of measurements was performed using a confocal parameter of 2 mm, with the same result.

B. Experiment II. Pressure dependence

Recordings of the THG light in the forward direction show that its spectrum broadens and shifts to the blue as the pressure is increased (Fig. 6, upper traces). The size of the shifts and the resulting line shapes are consistent with a theoretical fit of phase-matched third-harmonic generation.[15] The behavior of the ionization signal relative to the THG light is shown in the lower traces of Fig. 6. For these measurements, the laser intensity (attenuated to 35 kW) and the confocal parameter (90 μm) were fixed as the pressure was changed.

It should be noted that ionization signals taken at different pressures cannot be directly compared to yield the absolute ionization rates. This is because the gain of the ionization detector changes with pressure. As an aid to interpreting the data, the $4f$ resonance has been included in all of the scans.

In Fig. 6, there is no pressure for which the ionization signal is present exactly at the unperturbed $6s$ resonance. When the laser is tuned on resonance the sample is optically thick at ω_3, hence no ionization would be expected with the traveling-wave excitation in accordance with our theoretical treatment. As one scans away from resonance, eventually the detuning becomes large enough for the medium to become optically thin, and the "$6s$" ionization signal appears on the short-wavelength side of the resonance. The quotes are used to emphasize the fact that this type of enhancement, though due to the $6s$ state, will never appear on resonance. The observation of the "$6s$" ionization signal on the wings of the $6s$ resonance is directly correlated with the presence of the THG. At 1.5-Torr pressure, the "$6s$" and $4f$ ionization resonances are both prominent when the peak of the THG spectrum is close in

energy to the 6*s* state. At 3 Torr, the strength of the "6*s*" ionization is drastically reduced, and by 6.75 Torr, when the THG spectrum has shifted completely off the resonance line, the ionization signal has vanished completely. Note that as the THG overlaps in frequency with the 4*f* resonance, the vuv intensity is slightly quenched. This is consistent with the behavior reported earlier by Miller *et al.*[4] and is due to the two-photon absorption channel to the 4*f* state involving one vuv photon and one laser photon. The decrease in the transmitted THG intensity at 10 Torr is caused by absorption (at this pressure, the absorption depth is shorter than the length of the cell). On the other hand, the observed decrease at 0.5 Torr is caused by lower atomic density yielding less THG. Overall the strong pressure dependence of the "6*s*" is consistent with the expected behavior of the MPI if channel 1′ dominates the ionization pathways.

C. Experiment III. Confocal parameter dependence

In the four scans shown in Fig. 7, the upper curves depict the THG signal and clearly show that shortening the confocal parameters (shortening the focal lengths) while the pressure is held fixed (at 1.5 Torr) shifts the phase-matching peak closer to the 6*s* state. Physically, a sharper focusing angle changes the effective phase matching so that THG is maximized closer to the resonance line.

The dependence of the 4*f* and "6*s*" ionization resonances on the confocal parameter at a fixed pressure (1.5 Torr) is depicted in the lower curve. The laser power is fixed at 35 kW. *At no time does the vuv or the ionization signal overlap the unperturbed resonance position.* The relatively constant behavior of the 4*f* resonance signal can be explained by noting that enhanced ionization resulting from the increasing laser intensity within the focal volume, as the focal length shortens, is offset by a decrease in the excitation volume. In contrast, the dramatic feature in these scans is the tremendous enhancement of the "6*s*" ionization signal with shorter confocal parameters. The enhancement of the "6*s*" is clearly not an intensity effect due to tighter focusing but is due to the nearby 6*s* resonance. Therefore, at the lowest pressures where the THG is generated closest to the unperturbed resonance, the ionization signal is strongest. Note that for the 30-μm confocal parameter, the absorption depth at ω_3 is shorter than the length of the cell but longer than the *effective* sample length (i.e., the confocal parameter). This condition tends to maximize the ionization signal while reducing the observed vuv signal since this signal is absorbed before leaving the cell. Again, the "6*s*" resonance is consistently broad at all three intensities where it is still observable and does not exhibit a typical asymmetric Stark profile. Overall, the behavior of the "6*s*" ionization signal is consistent with the expected behavior of I_3 due to changing the confocal parameter [Eq. (14)].

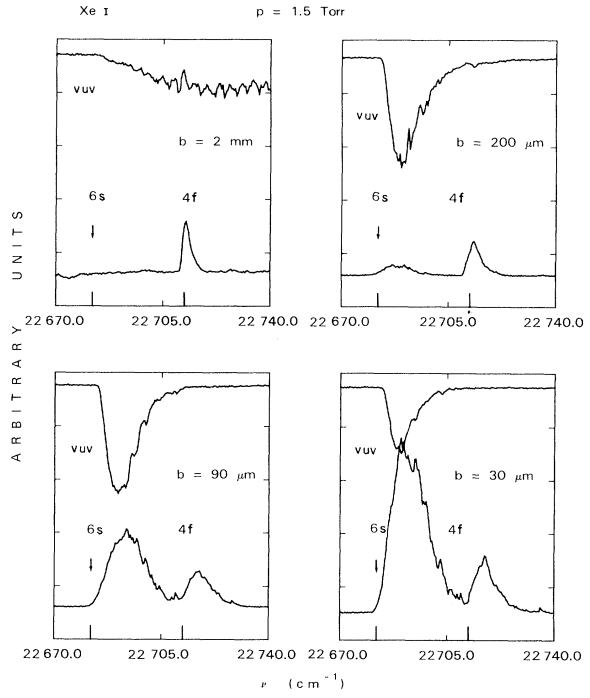

FIG. 7. Confocal parameter dependence of THG (upper curve) and ionization signal (lower curve) vs laser energy in cm^{-1}. The tick marks below indicate the position of the unperturbed 6*s* and 4*f* resonances. PMT voltage and ionization voltage are constant for all scans except that taken with the 2-mm confocal parameter.

D. Experiment IV. Power dependence

The confocal parameter results (Fig. 7) suggest that the 4*f* and "6*s*" states have different power dependences. This was confirmed by carefully measuring the signal strengths of both the 4*f* and "6*s*" as the laser intensity was attenuated with calibrated neutral density filters. For these measurements the pressure and confocal parameter were held fixed at 0.8 Torr and 200 μm, respectively. By this means, one obtains power dependences which vary roughly as the fourth and fifth power of the intensity for the 4*f* and "6*s*" resonances, respectively (Fig. 8). Thus ionization through the 4*f* state involves a lower-order power dependence than that at the "6*s*" state. Collisional ionization through an associative ionization channel

$$Xe^*(4f)+Xe \rightarrow Xe_2^+ + e^- \tag{15}$$

is energetically favorable[20] and will likely account for this power dependence. However, these data do not preclude the possibility that the one-photon transition from the 4*f* state to the continuum might be saturated at these powers.

E. Experiment V. Double-cell measurements

We used the measurements from the double-cell configuration [Fig. 4(c)] to correlate the observed vuv signal with the measured ionization signal. The purpose of these measurements was to study the behavior of three-photon ionization (one vuv photon plus two laser photons) while eliminating Stark broadening and direct five-photon ionization in cell 2. We first adjusted the laser intensity in cell 2 to a value of 10—100 times less than that used for recording Figs. 6 and 7; then we established that no ionization signal was generated in cell 2 if cell 1 was completely evacuated so that no THG occurred. This demonstrates that the five-photon ionization is negligible in cell

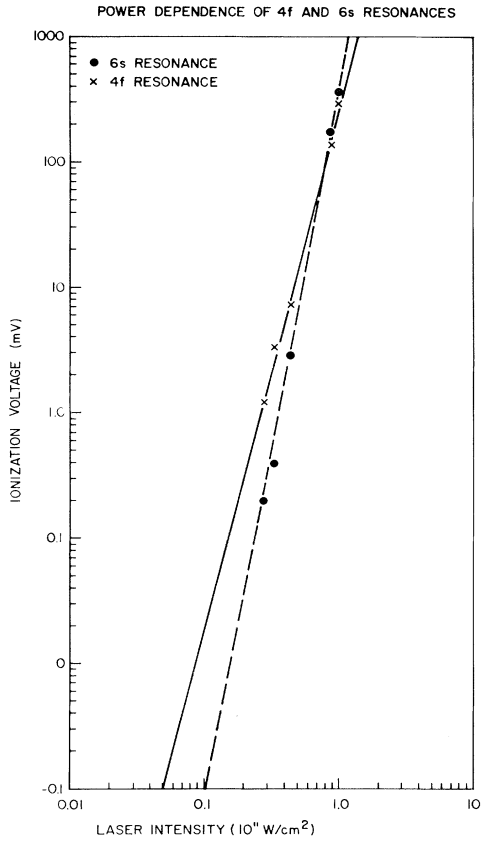

FIG. 8. Intensity dependence of the ionization signal showing that excitation via the "6s" transition has a fifth-order intensity dependence compared with the $4f$ transition which has an intensity dependence of I^4.

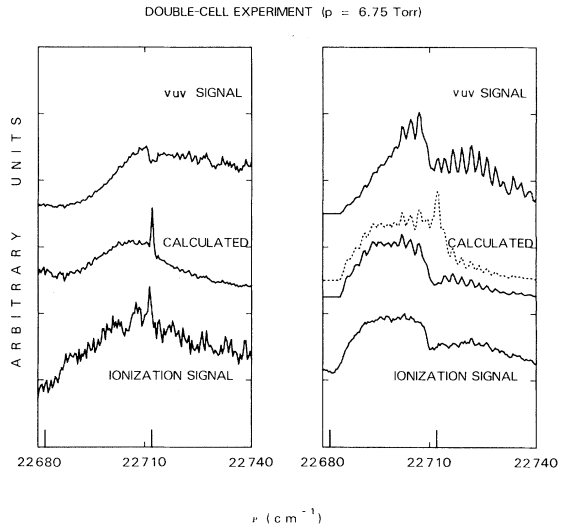

FIG. 9. Comparison of the measured vuv signal (upper curves) with the measured ionization signal (lower traces) shows discrepancies from one line shape to the other. Weighting the vuv signal with the expected resonance-enhancement factors gives much better agreement as shown in the center curves.

2. Adding gas to cell 1 generated vuv which caused ionization in cell 2. We found that shifting the third-harmonic spectrum to the blue by raising the pressure in cell 1 caused the measured ionization signal spectrum in cell 2 to track the vuv spectrum. The ionization and vuv spectra differed in that the ionization signal was stronger relative to the measured vuv signal at frequencies adjacent to the $6s$ resonance. This reflects the resonance enhancement of the ionization process via the $6s$ state.

An example of vuv and ionization spectra taken with the pressure in both cells fixed at 6.75 Torr is shown in Fig. 9. The upper curve is the vuv signal while the lower curve shows the ionization signal. (The curve in the middle is calculated from the vuv signal, as will be discussed below.) Although both scans are simultaneously generated, the line shapes of the vuv and ionization signals appear to be strikingly different in that the leading edge of the vuv signal rises more slowly than that of the ionization signal. In the left side of Fig. 9, one also observes an enhancement in the ionization at the position of the $4f$ due to the resonant two-photon absorption to this state. In the right side of Fig. 9 one observes a dip at the position of the $4f$ state apparently due to enhancement of a radiative decay channel (probably amplified spontaneous emission to the $6d$ state). Interference effects imposed on the vuv signal with a periodic 2.6-cm^{-1} oscillation are clearly seen in this figure. These are caused by interference between the third-harmonic field generated in cell 1 and the third-harmonic field generated in the LiF window. Using extrapolated values for the index of refraction of lithium fluoride, we estimate a 3.4-cm^{-1} periodicity for such a process, which is close to our experimental value. These oscillations are also evident on the measured ionization signal, although with less contrast. Using Eq. (14), the measured vuv intensity I_3, and the fact that in xenon the density of final states $\rho(5\omega_1)$ is slowly varying, one can calculate a good fit to experiment (middle curve in Fig. 9). Only the most important terms are kept when summing over k and k'; this reduces the expression to a sum of two Lorentzian terms which physically represent different resonance-enhanced ionization channels via the $6s$ and $4f$ states.

Multiplying the recorded vuv signal by

$$W_{fg}^{(3)}(\omega_3,2\omega_1) = \left[\frac{K_1}{|\omega_{n'g}-\omega_3|^2}+\frac{K_2}{|\omega_{pg}-\omega_3-\omega_1|^2}\right]I_3\,, \quad (16)$$

where $|n'\rangle \equiv |6s\rangle$ and $|p\rangle \equiv |4f\rangle$, produces a closer fit to the ionization spectrum as indicated by the center trace of the figure. It is important to realize that channels 1′ and 1‴ involve completely different intermediate and final states and are therefore not coherently related. This has been handled in Eq. (16) by dropping the cross terms (i.e., summing the matrix elements after squaring). The calculation for the left side of Fig. 9 involved a five-parameter fit, where two of the parameters I_3 and Γ_{pg} are taken from the data curves in the left side of Fig. 9. The other

parameters, the scaling constants K_1, K_2, and $\Gamma_{n'g}$ were chosen to give the best fit. This fit is obtained for $\Gamma_{n'g}/2\pi c = 16$ cm^{-1}. (From our estimated THG powers, we calculated a value of 9 cm^{-1} for the power-broadened linewidth.) The fit is not perfect because the THG intensity changes rapidly with the laser detuning from resonance. Hence, the linewidth $\Gamma_{n'g}/2\pi c$ will not be constant at 16 cm^{-1} but is expected to exhibit a strong dependence on the THG intensity.

The analogous, five-parameter fit to the data in the right side of Fig. 9 (dotted line), shows a discrepancy in the region near the $4f$ resonance, because we have not included a term for the radiative loss from $4f$ state. Including a loss term, $\exp(-az)$, gives better agreement with the observed ionization signal (solid line). The attenuation from this loss term also reduces the contrast in the vuv 2.6-cm^{-1} oscillatory structure.

V. DISCUSSION

A. 6s state

In the theoretical treatment, we have found that systematic inclusion of the important channels leading both into and out of the $6s$ resonance in Xe accounts for the absence of resonance enhancement at the $6s$ state when the sample is optically thick and traveling-wave excitation is used. The two fields $E_{\text{eff}}(3\omega_1,\vec{r},t)$ and $E(\omega_3,\vec{r},t)$, drive the transition 180° out of phase so that there is no dipole induced at the transition. This is seen in the transition rate calculation [Eq. (4)] as a destructive interference between the two coherently related pathways (channels 1 and 1′) going into the resonance. A more physical interpretation of this effect in terms of the two-state vector model for an ensemble of states is presented in an earlier paper.[7] Overall, the data we present are completely consistent with the expectations of this physical model.

Our experimental findings are also in quantitative agreement with the findings of Glownia and Sander[5] in that we can produce resonance-enhanced ionization *at* the $6s$ state with a standing-wave laser excitation. In general, our data are consistent with the findings of Miller *et al.*[4]; moreover, our data clearly show that the resonance signal which disappears is not that of the direct five-photon absorption at the $6s$ resonance position. We have shown that the pressure at which the "$6s$" ionization disappears is strongly correlated with the tightness of the focus. In general, we have observed both the "$6s$" and the $4f$ ionization resonances at low pressures and find that as the gas pressure is increased, the "$6s$" ionization signal disappears.

Earlier, we emphasized that the preceding calculation is for the idealized conditions of low laser power and low atomic density. Although the contributions from the effects of high laser power and high atomic density are not explicitly included in our calculation of the MPI transition rate, Eq. (4) clearly shows that the *depolarization effect* at ω_3 is independent of both pressure and power broadening of the atomic linewidth.

Most of the other published results on MPI in Xe were taken at intensities which were at least an order of magnitude lower than the intensities we used. Stark shifts and power broadening were negligible in these other experiments. In contrast to these earlier studies and our double-cell measurements, the spectra that we publish in Figs. 6 and 7 were recorded under conditions where the power broadening is severe. All of our data were carefully calibrated to show the behavior of both the "$6s$" and $4f$ resonance relative to their unperturbed resonance positions. From this one can see that the intensities in many of the spectra are strong enough to completely Stark shift the four-photon $4f$ resonance away from its unperturbed position. Even with the atomic wave functions grossly distorted by the intense optical electric fields, in the optically thick, traveling-wave case, resonance-enhanced ionization via the $6s$ state is *still* suppressed by the dynamic cancellation of the two driving fields in Eq. (4b). This result confirms that our treatment in Sec. II, which is known to be valid for low intensities, can also be generalized for high intensities. This cancellation no longer takes place, however, when the detuning from resonance is large enough for the gas to become optically thin; channel 1′ begins to dominate, and the observed "$6s$" ionization signal on the wings of the $6s$ resonance tracks the vuv signal with an accompanying enhancement from the nearby $6s$ state.

Some discussion of the incoherent channels is appropriate at this point. In this paper, we have explicitly avoided treating the damping terms because we believe that over the range of pressures relevant to our experiments they make a negligible contribution. On the other hand, the data published by Miller *et al.*[4] cover a wide range of pressures (from 1 mTorr to 300 Torr). At the extreme high pressures where collisional effects are no longer negligible, they still observe a suppression of the resonance-enhanced ionization via the $6s$ state. This is consistent with our assumption that the collisional terms will enter into the numerator and denominator of Eq. (7) in such a manner as to preserve the normalization.

An experiment by Faisal *et al.*[21] confirms our assumption that incoherent channels (collisions, radiative fluorescence, etc.) can be treated in Eq. (4) as part of the phenomenological damping term Γ. Faisal *et al.*[21] have reported observation of incoherent radiative fluorescence decay from the $6s$ state after population by three-photon absorption. This was accomplished by detecting the fluorescence 90° to the laser beam. In such an experiment, if the destructively interfering channels suppress the polarization on this transition, this 90° fluorescence signal should also vanish. In their experiment, the laser was carefully aligned to skim the surface of the fluorescence exit window of the cell. At very low pressures, the radiative fluorescence at 147 nm was clearly observable, whereas above roughly 50 mTorr, there was no sign of fluorescence.[17] They speculated that the "fluorescence is resonantly trapped and reduced due to the quenching of excited atoms by gas impurities," even though the laser was adjusted to skim within 50 μm of the window, a geometry for which *total* extinction due to quenching collisions was unlikely [some photons would still to "leak" out to the photomultiplier tube (PMT)]. In fact, the fluorescent signal vanishes because there is no excitation of the $6s$ state (beyond an absorption depth into the sample).

Prior *et al.*[21] have recently calculated the effects of collisional dephasing on coherent four-wave mixing processes. In the absence of collisions, their analysis shows that significant contributions from near-resonant terms in the

nonlinear susceptibility are canceled by destructive interference among coherently driven channels. However, this perfect cancellation can be destroyed by collisions, thereby producing extra resonances between unpopulated states. These predictions have been confirmed by experiments at pressures above 5 Torr. These results raise questions about the validity of our assumption that collisional effects can be neglected in our treatment of MPI and THG. However, Prior *et al.*[22] have addressed the particular case of nonlinear optical mixing where the frequencies were near resonance with transitions between unpopulated excited states. In our case, we are far removed from any such resonances so that the time-ordered diagrams and the corresponding collisional effects associated with them are negligible.

B. 4*f* state

The 4*f* resonance has been used as the reference against which the behavior of the 6*s* state is calibrated. Such use is valid even though we have noted that the 4*f* ionization signal displays a lower power dependence, probably due to a different ionization mechanism. The 4*f* resonance differs from the case of the 6*s* resonance because there is no dipole coupling from the 4*f* state to the ground state; hence THG cannot occur. The possible channels through the 4*f* state [Figs. 1(c) and 1(d)] are thus 1″ five-photon ionization; 2″ four-photon absorption followed by collisional scattering, and the corollary channels 1‴ and 2‴ where the excitation to the 4*f* state involves two-photon absorption $(\omega_3+\omega_1)$. Note that channels 1‴ and 2‴ must be included here because the nonresonant 6*s* state can still generate a THG wave which contributes to ionization. With a high-lying state such as the 4*f*, two incoherent loss channels are possible: (1) radiative fluorescence to lower-lying *d* states and (2) the associative ionization process described in Eq. (15). The contribution of associative ionization to the total ionization signal can lower the order of the power dependence.

The scans in Fig. 6 present qualitative evidence that the two-photon channel $(\omega_3+\omega_1)$ to the 4*f* state makes a major contribution to the ionization signal. At low pressures, the resonance at the 4*f* appears both Stark broadened and Stark shifted away from the unperturbed resonance position indicated by the tick mark in the figure. At the higher pressures (6.75 and 10 Torr) when the THG overlaps the 4*f* resonance, the line shapes of the vuv and ionization signals are modified by the presence of this resonance. The vuv intensity is attenuated by two-photon $(\omega_3+\omega_1)$ resonance absorption into the 4*f* state, and the 4*f* resonance-enhanced ionization signal, although it still maintains a long blue tail, now rises sharply at the position of the 4*f* resonance. The observation of ionization *at* the 4*f* resonance is a result of the strong two-photon resonance-enhanced ionization occurring in the volume outside the focal region where the field intensities (and correspondingly the Stark shifts) are relatively small. This implies that the ionization probability for channels 1‴ and 2‴ is still large, even at the lower laser powers.

We have observed experimentally that two-photon absorption $(\omega_3+\omega_1)$ to the 4*f* state is an important excitation channel. A simple calculation confirms that this is generally what one expects. That is, comparing the ionization rates for the two different channels (1″ and 1‴ or 2″ and 2‴) shows that the ionization via a harmonically generated photon will often be the dominant ionization term. The ratio of the ionization rates via the 4*f* state are

$$\frac{W_{fg}^{(3)}(\omega_3+2\omega_1)}{W_{fg}^{(5)}(5\omega_1)}=\left|\frac{4\pi N_0 e^2 x_{rg}x_{gn'}x_{n'm}}{\hbar(\omega_{n'g}-\omega_3)(\epsilon_1-\epsilon_3)x_{rm}}\right|^2 =\frac{W_{fg}^{(2)}(\omega_3+\omega_1)}{W_{fg}^{(4)}(4\omega_1)}\,, \tag{17}$$

where the state $|r\rangle$ represents the *d* states which couple to the 4*f* state and $|n'\rangle$ denotes the $|6s\rangle$ state as usual. One observes that the above ratio depends on the density N_0, the detuning $\omega_{n'g}-\omega_3$, and the phase-mismatch factor $\epsilon_1-\epsilon_3$. For a detuning of 92 cm^{-1}, a pressure of 1 Torr, an oscillator strength $f_{n'g}=2\omega_3 m\,|x_{n'g}|^2/\hbar=0.27$ and a relative phase mismatch $|\Delta k/k|$ of 10^{-5}, the ratio becomes roughly

$$\frac{W_{fg}^{(3)}(\omega_3+2\omega_1)}{W_{fg}^{(5)}(5\omega_1)}\cong 7\left|\frac{x_{rg}}{x_{n'g}}\right|^2\left|\frac{x_{n'm}}{x_{rm}}\right|^2. \tag{18}$$

For xenon, the major contribution comes from $|m\rangle=|g\rangle$ (since there are no real states intermediate between $|6s\rangle$ and $|g\rangle$), so that the ratio of the matrix elements reduces to 1. This is a situation where three-photon ionization dominates.

Thus, inside of the focal volume, we estimate that channels 1‴ and 2‴ ionize more efficiently than channels 1″ and 2″. Outside of the focal volume channel 1‴ (2‴) will continue to dominate the ionization pathways because the three-photon ionization probability has only a second-(first)-order dependence on the laser intensity *outside* of the focus and is linearly dependent on the amount of THG generated *within* the focal volume. Contributions to the ionization in the volume outside of the focus from channel 1″ (2″) are much smaller since they have higher-order dependencies on the laser intensity. More generally, this suggests that once the first odd resonance produces harmonic generation, the ionization of higher-lying states could be dominated by channels which include the absorption of these harmonics. Since these higher harmonics ionize more efficiently than the fundamental, it is possible that they might also play a heretofore unrecognized role in saturating transitions to the continuum.

VI. CONCLUSIONS

The major impetus of this paper has been to highlight the complementary nature of the two nonlinear phenomena, multiphoton ionization and third-harmonic generation. Having presented a general theoretical framework from which the ionization behavior can be predicted, we conclude with the following observations. A traveling-wave excitation which is three-photon resonant with the first excited state will generate a harmonic field which drives the transition 180° out of phase; but the dynamic balance maintained between the driving wave and the THG wave can be destroyed by using standing-wave excitation. This result, for THG in an optically thick absorber, is probably one of the simplest cases for calculations and lends itself nicely to easy physical interpretation. It correspondingly lays the ground work for the treatment of more complex cases involving parametric generation. We have seen that

interference effects between different excitation channels affects the presence of resonance enhancement of the ionization signal as well as the position and line shape of the resulting excitation. These findings are expected, in turn, to influence the future interpretation of MPI spectra.

APPENDIX

Reintjes[13] has calculated a general expression for nth harmonic generation by assuming that the fields at the fundamental $E(\omega_1)$ and the nth harmonic $E(\omega_n)$ make the only important contribution to the total polarization at ω_n. In fact we realize that, if the fields are large enough to generate significant nth harmonic, one must include the contributions of all of the lower harmonics [$(n-2)$th, $(n-4)$th, etc.] to the driving polarization.

If one treats the generation of the fifth harmonic, for example, the total polarizations at ω_3 and ω_5 are

$$P^{\text{tot}}(\omega_3)=\chi^{(1)}(\omega_3)E(\omega_3)+\chi^{(3)}(3\omega_1)E^3(\omega_1)+\chi^{(3)}(\omega_5-2\omega_1)E(\omega_5)[E^*(\omega_1)]^2 \tag{A1}$$

and

$$P^{\text{tot}}(\omega_5)=\chi^{(1)}(\omega_5)E(\omega_5)+\chi^{(3)}(\omega_3+2\omega_1)E(\omega_3)E^2(\omega_1)+\chi^{(5)}(5\omega_1)E^5(\omega_1) \tag{A2}$$

with

$$\chi^{(1)}(\omega_3)\equiv\frac{N_0e^2|x_{n'g}|^2}{\hbar(\omega_{n'g}-\omega_3)},$$

$$\chi^{(3)}(3\omega_1)\equiv\frac{N_0e^4}{\hbar^3}\frac{x_{gn'}x_{n'm}x_{mm'}x_{m'g}}{(\omega_{n'g}-3\omega_1)(\omega_{mg}-2\omega_1)(\omega_{m'g}-\omega_1)},$$

$$\chi^{(3)}(\omega_5-2\omega_1)\equiv\frac{N_0e^4}{\hbar^3}\frac{x_{gn'}x_{n'k}x_{kf}x_{fg}}{(\omega_{n'g}-\omega_3)(\omega_{kg}-4\omega_1)(\omega_{fg}-5\omega_1)}, \tag{A3}$$

$$\chi^{(3)}(\omega_3+2\omega_1)\equiv\frac{N_0e^4}{\hbar^4}\frac{x_{gf}x_{fk}x_{kn'}x_{n'g}}{(\omega_{fg}-5\omega_1)(\omega_{kg}-4\omega_1)(\omega_{n'g}-\omega_3)},$$

$$\chi^{(5)}(5\omega_1)\equiv\frac{N_0e^6}{\hbar^5}\frac{x_{gf}x_{fk}x_{kn'}x_{n'm}x_{mm'}x_{m'g}}{(\omega_{fg}-5\omega_1)(\omega_{kg}-4\omega_1)(\omega_{n'g}-3\omega_1)(\omega_{mg}-2\omega_1)(\omega_{m'g}-\omega_1)}.$$

The fields $E(\omega_1)$, $E(\omega_3)$, and $E(\omega_5)$ are those of the fundamental, third harmonic, and fifth harmonic, respectively. It is important to note that the fundamental $E(\omega_1)$ is a focused Gaussian beam, which therefore exhibits strong spatial dependences. Although this dependence is not included in any of the above expressions, it is assumed for all of the fields.

When the medium is optically thick at ω_3, the fields $E(\omega_1)$, $E(\omega_3)$, and $E(\omega_5)$ tend to self-adjust so that $P^{\text{tot}}(\omega_3)=0$. Hence

$$E(\omega_3)=-\frac{\chi^{(3)}(3\omega_1)E^3(\omega_1)}{\chi^{(1)}(\omega_3)}-\frac{\chi^{(3)}(\omega_5-2\omega_1)E(\omega_5)[E^*(\omega_1)]^2}{\chi^{(1)}(\omega_3)} \tag{A4}$$

and

$$P^{\text{tot}}=\frac{\chi^{(1)}(\omega_5)\chi^{(1)}(\omega_3)-\chi^{(3)}(\omega_3+2\omega_1)\chi^{(3)}(3\omega_1)|E(\omega_1)|^4}{\chi^{(1)}(\omega_3)}E(\omega_5)+\frac{\chi^{(5)}(\omega_5)\chi^{(1)}(\omega_3)-\chi^{(3)}(\omega_3+2\omega_1)\chi^{(3)}(\omega_5-2\omega_1)}{\chi^{(1)}(\omega_3)}E(\omega_1)^5. \tag{A5}$$

The coefficient of the first term in Eq. (A5) is just the polarization contribution to the index of refraction

$$\epsilon_5=1+4\pi\left[\chi^{(1)}(\omega_5)-\frac{\chi^{(3)}(\omega_3+2\omega_1)\chi^{(3)}(3\omega_1)}{\chi^{(1)}(\omega_3)}|E(\omega_1)|^4\right] \tag{A6}$$

which is modified by a second-order Kerr term.

The second term in Eq. (A5) is the driving polarization by which the fifth harmonic is generated. Substituting Eqs. (A3) for the susceptibilities in Eq. (A5) shows that the coefficients of this second term sum to zero. This means that no fifth harmonic is generated as long as the fields are dynamically balanced to destroy the polarization at ω_3.

*Present address: Hughes Research Laboratory, Malibu, California 90265.

†Present address: K. Onnes Laboratory, Leiden, The Netherlands.

[1]P. M. Johnson, Acc. Chem. Res. 13, 20 (1980); H. B. Bebb and A. Gold, Phys. Rev. 143, 1 (1966).

[2]K. Aron and P. M. Johnson, J. Chem. Phys. 67, 5099 (1977).

[3]R. N. Compton, J. C. Miller, A. E. Carter, and P. Kruit, Chem. Phys. Lett. 71, 87 (1980).

[4]J. C. Miller, R. N. Compton, M. G. Payne, and W. W. Garrett,

Phys. Rev. Lett. 45, 114 (1980); J. C. Miller and R. N. Compton, Phys. Rev. A 25, 2056 (1982).

[5]J. H. Glownia and R. K. Sander, Phys. Rev. Lett. 49, 21 (1982).

[6]M. G. Payne, W. R. Garrett, and H. C. Baker, Chem. Phys. Lett. 75, 468 (1980); M. G. Payne and W. R. Garrett, Phys. Rev. A 26, 356 (1982).

[7]D. J. Jackson and J. J. Wynne, Phys. Rev. Lett. 49, 543 (1982).

[8]D. R. Grischkowsky, Phys. Rev. A 14, 802 (1976).

[9]J. F. Ward, Rev. Mod. Phys. 37, 1 (1965).

[10]N. Bloembergen, *Nonlinear Optics* (Benjamin, New York, 1964), pp. 74—85.

[11]From our measurements we estimate that the two-photon ionization cross section out of the 6*s* state at 440.8 nm is greater than 10^{-24} cm^4/W; the one-photon ionization cross section at 147 nm has been calculated to be 10^{-20} cm^2. With a laser power of 5×10^{11} W/cm^2 and an estimated vuv power of 5×10^{6} W/cm^2, ionization via channels 1 and 1′ is expected to be 12 orders of magnitude larger than that via channels 4 and 4′; see D. Ton-That and M. R. Flannery, Phys. Rev. A 15, 517 (1977); K. J. McCann and M. R. Flannery, Appl. Phys. Lett. 31, 599 (1977).

[12]H. Kogelnik and T. Li, Appl. Opt. 5, 1550 (1966).

[13]The absorption cross section at the fifth harmonic is 6.5×10^{-17} cm^2 [H. Egger, R. T. Hawkins, J. Bokor, H. Pummer, M. Rothschild, and C. K. Rhodes, Opt. Lett. 5, 282 (1980)]. In addition, at small detunings from resonances, when the beam is focused into the center of an "infinite" medium, the amplitude of the third-harmonic field is at least an order of magnitude larger than the fifth-harmonic amplitude [J. Reintjes, Appl. Opt. 14, 3889 (1980)].

[14]R. P. Feynman, F. L. Vernon, Jr., and R. W. Hellwarth, J. Appl. Phys. 28, 49 (1957); D. Grischkowsky, Phys. Rev. A 7, 2096 (1973).

[15]J. F. Ward and G. H. C. New, Phys. Rev. 185, 57 (1969); G. C. Bjorklund, IEEE J. Quantum Electron. QE-11, 287 (1975); C. R. Vidal, Appl. Opt. 19, 3897 (1980).

[16]P. F. Liao and J. E. Bjorkholm, Phys. Rev. Lett. 34, 1 (1975).

[17]R. Wallenstein and H. Zacharias (private communication).

[18]P. Esherick (private communication).

[19]J. F. Lam and R. L. Abrams, Phys. Rev. A 26, 1539 (1982).

[20]R. S. Mulliken, J. Chem. Phys. 52, 5170 (1970).

[21]F. H. M. Faisal, R. Wallenstein, and H. Zacharias, Phys. Rev. Lett. 39, 1138 (1977).

[22]Y. Prior, A. R. Bogdan, M. Dagenais, and N. Bloembergen, Phys. Rev. Lett. 46, 111 (1981).